



**HAL**  
open science

## High temperature oxidation of a Cu-Ni – based cermet: kinetic and microstructural study

Fabien Rioult, Michèle Pijolat, Françoise Valdivieso, Marie-Agnès  
Prin-Lamaze

### ► To cite this version:

Fabien Rioult, Michèle Pijolat, Françoise Valdivieso, Marie-Agnès Prin-Lamaze. High temperature oxidation of a Cu-Ni – based cermet: kinetic and microstructural study. *Journal of the American Ceramic Society*, 2006, 89 (3), pp.996-1005. 10.1016/j.corsci.2009.01.019 . hal-00409342

**HAL Id: hal-00409342**

**<https://hal.science/hal-00409342>**

Submitted on 6 Aug 2009

**HAL** is a multi-disciplinary open access archive for the deposit and dissemination of scientific research documents, whether they are published or not. The documents may come from teaching and research institutions in France or abroad, or from public or private research centers.

L'archive ouverte pluridisciplinaire **HAL**, est destinée au dépôt et à la diffusion de documents scientifiques de niveau recherche, publiés ou non, émanant des établissements d'enseignement et de recherche français ou étrangers, des laboratoires publics ou privés.

## High temperature oxidation of a Cu-Ni – based cermet: kinetic and microstructural study

FABIEN RIOULT<sup>A</sup>, MICHELE PIJOLAT<sup>A,1</sup>, FRANÇOISE VALDIVIESO<sup>A</sup>, MARIE-AGNES PRIN-LAMAZE<sup>B</sup>

<sup>a</sup>LPMG CNRS UMR 5148, Centre SPIN, Ecole nationale supérieure des mines de Saint-Etienne, 42023 Saint-Etienne, France

<sup>b</sup>Alcan CRV, Centr'Alp, BP27, 38341 Voreppe, Cedex France

### Abstract

The oxidation of a cermet composed of nickel ferrite ( $\text{Ni}_x\text{Fe}_{3-x}\text{O}_4$ ), nickel oxide ( $\text{Ni}_y\text{Fe}_{1-y}\text{O}$ ) and Ni-Cu alloy ( $\text{Cu}_z\text{Ni}_{1-z}$ ) (with  $x=0.8$ ,  $y=0.84$  and  $z=0.44$ ) has been studied by thermogravimetry, at  $960^\circ\text{C}$ , under controlled oxygen partial pressure. The rate of oxidation increases with the oxygen partial pressure up to  $5.1 \cdot 10^3$  Pa, then it becomes independent of the oxygen pressure. This is due to the presence of the two copper oxides, CuO and  $\text{Cu}_2\text{O}$ , above this oxygen pressure. SEM observation of oxidized samples has shown that the oxidation mechanism involves both external and internal oxidation.

**Keywords:** cermet ; oxidation ; mechanisms ; diffusion ; interfaces.

### INTRODUCTION

Inert electrode materials have been investigated for use in aluminum production using the electrolysis process for many years. Currently, the Hall-Heroult process uses carbon anodes that are consumed during the process, releasing carbon dioxide. This is environmentally and economically disadvantageous for the aluminum production industry. Some non-consumable anodes have already been proposed such as copper-nickel-iron alloys<sup>1</sup>.

Many patents have been published in the last 20 years (see for example <sup>2-4</sup>), showing that cermet are good candidate materials for use as inert anodes in the aluminum electrolysis process, due to their combined properties of good conductance and resistance to oxidation. At temperatures as high as  $900-1000^\circ\text{C}$ , these materials must be resistant to corrosion, not only by the electrolytic bath, but also by oxygen and fluorides contained in the atmosphere. The present work is devoted to the study of the oxidation of a cermet composed of nickel ferrite, nickel oxide and Cu-Ni alloy, at  $960^\circ\text{C}$ , in which the electrical conductivity is due to both metallic and nickel ferrite phases. The metallic phase improves the mechanical properties, and the nickel oxide phase, the sintering during elaboration. The evolution of the various phases and the effect of oxygen pressure on the oxidation kinetics have been investigated in order to determine the reaction mechanisms.

First, we present thermogravimetric measurements at  $960^\circ\text{C}$  under controlled oxygen pressure in the range  $10^2 - 10^5$  Pa. This temperature has been chosen due to the Hall-Heroult electrolysis process requirements. The influence of oxygen pressure on the rate of oxidation was determined by means of sudden changes in  $P_{\text{O}_2}$  in the course of oxidation experiments<sup>3</sup>. Then, SEM observations have been obtained from several samples oxidized under various conditions. The composition of the phases has been followed with EPMA. The experimental results have been explained on the basis of a mechanism involving both external oxidation and internal oxidation. Diffusion of copper towards the surface and diffusion of oxygen into the material can account for the rate of weight gain measured in the isothermal experiments and for the influence of oxygen pressure.

### Samples and Experimental procedure

#### Samples

---

<sup>1</sup> mpijolat@emse.fr

Corrosion Science, 2009, 51(4), 752-760, [doi:10.1016/j.corsci.2009.01.019](https://doi.org/10.1016/j.corsci.2009.01.019)  
Cermets composed of nickel ferrite ( $\text{Ni}_x\text{Fe}_{3-x}\text{O}_4$ ), nickel oxide ( $\text{Ni}_y\text{Fe}_{1-y}\text{O}$ ) and nickel-copper alloy ( $\text{Cu}_z\text{Ni}_{1-z}$ ) was made using a powder metallurgy process. EPMA was used to determine the chemical composition of the oxide phases and X-Ray diffraction was used to determine that of the metallic phase:  $x=0.8$ ;  $y=0.84$ ;  $z=0.44$ . The weight proportion of each phase, estimated by X-ray diffraction and the Rietveld method, is  $44 \pm 1$  %wt for the nickel ferrite,  $21 \pm 2$  %wt for the nickel oxide and  $35 \pm 4$  %wt for the alloy.

Figure 1 shows the distribution of the phases in the material: metallic particles (label a) are more or less spherical with a mean diameter of 20  $\mu\text{m}$  and are surrounded by the nickel ferrite phase (label b) which is the only phase that percolates in all the material. The rest is made up of the nickel oxide phase (label c) and porosity (measured to be less than 5% of the volume).

The cermets were provided in the form of cylindrical bars with a diameter of approximately 15 mm. We resized them to 9 mm and sliced them to approximately 0.5 mm thick disks. This geometry was chosen to fit in the thermogravimetric analyzer furnace and to make it possible to neglect the contribution of the oxidation of the sides of the disks to the whole weight gain.

### Thermogravimetric analysis

All oxidation experiments were performed in, either symmetric or asymmetric thermogravimetric analyzers (SETARAM TGA24 and TGA92 respectively), according to the following procedure: the temperature was raised to 960°C (10°C/min) under flowing argon at atmospheric pressure (10 L/h) in order to prevent the material from oxidizing (argon contains less than 10 ppb of oxygen and oxidation under argon can be neglected), then at 960°C, a flowing mixture of Ar and O<sub>2</sub> was introduced. The partial pressures of the gases being controlled by flowmeters (BROOKS, 5850E), the oxygen partial pressure was fixed in the range of  $10^2 - 10^5$  Pa. At the end of the oxidation experiment performed under isobaric and isothermal conditions, the temperature was programmed to decrease as fast as possible (approximately 30°C/min) in order to avoid changing the microstructure during the cool-down. The oxidation rate was determined by plotting the weight gain per unit surface area of the sample ( $1.27 \times 10^{-4} \text{m}^2$ ).

Abrupt changes in  $P_{\text{O}_2}$  were applied during the isotherm at 960°C, by varying the oxygen and argon flowrates (the total flowrate remaining constant).

### Gold marker sputtering

Gold markers were used on a few samples in order to localize the position of the initial surface after oxidation<sup>4</sup>. This method allows us to determine if the growth of the oxide layer occurs outwards or inwards. Gold is chosen as a marker because it is inert in the oxidation conditions of oxygen pressure and temperature. Gold droplets were deposited on the initial surface using a sputter coater (BALZERS SCD 050).

### SEM and EPMA

All of the oxidized samples observed with a SEM or EPMA have been prepared using the same process. Cermets disks were cut in half with a diamond disk and coated with a phenolic hot mounting resin with carbon filler. Then they were polished with 180-grains/cm<sup>2</sup> SiC-papers to 1 micron felt using decane and diamond polishing suspensions respectively. Then samples were cleaned with ethanol. The SEM observations were made using a Zeiss DSM 950 and EPMA analysis using a CAMECA SX100.

### SIMS Analysis

A sample has been oxidized in the thermogravimetric analyzer (SETARAM TGA24) in a flowing mixture of 990 hPa of argon and 10 hPa of isotopic <sup>18</sup>O<sub>2</sub> for 24 hours (according to the procedure detailed in the section “thermogravimetric analysis”). After cooling, the sample was cut in two parts with a diamond disk and coated with a low-pressure epoxy resin (Varian Torr Seal). Then, it was polished as described previously for SEM and EPMA analysis.

SIMS observations were obtained using a CAMECA NanoSIMS 50. The measurements of <sup>18</sup>O, <sup>16</sup>O, (Ni + O), (Fe + O) and (Cu + O) were performed in imaging mode (100x100  $\mu\text{m}^2$ ,

Corrosion Science, 2009, 51(4), 752-760, [doi:10.1016/j.corsci.2009.01.019](https://doi.org/10.1016/j.corsci.2009.01.019) 65x65  $\mu\text{m}^2$ , 35x35  $\mu\text{m}^2$ ). The primary ion beam used was a 200-300 nm  $\text{Cs}^+$  (16 keV). A mass resolution of  $M/dM = 5000$  has been used to avoid interferences ( $^{18}\text{O}/^{16}\text{OH}_2$ ). On the sample, a measurement of the  $^{18}\text{O}/^{16}\text{O}$  ratio was performed at the center of the disk (non-oxidized zone) to check that the measurement was correct and equal to the ratio on the earth (0,002). Then, several series of images were acquired on the oxidized zones. All of the images are presented using a logarithmic color scale going from black (signal = 0) to red (99% of the maximum signal).

## Results

### Mass gain versus time

Figure 2 represents a typical oxidation curve, giving the weight gain versus time, at 960°C in  $10^5$  Pa of oxygen. Two different regimes can be observed on the curve. In Part 1, the mass gain is fast and the reaction rate decreases rapidly. In Part 2, which extends above a mass gain higher than 15 g/m<sup>2</sup>, the rate of oxidation is nearly constant. Part 1 may correspond to the oxidation of the Cu-Ni alloy particles, which are located at the surface of the sample and not protected by the nickel ferrite phase. Only Part 2 will be described in this paper, since it represents the long-term behavior of the material and is the most interesting part for lifetime prediction. The kinetics of oxidation is directly linked with the rate-limiting step and the dimension of the zone where it takes place. The linearity of the weight gain curve means that the dimension of this zone is nearly constant. This can happen when the rate-limiting step is an interface reaction of constant surface or a diffusion of species through an oxide layer of constant thickness. Although the geometry of this cermet is complex, a rate-limiting step of this kind would explain a linear mass gain curve.

### Oxygen partial pressure influence

The influence of oxygen pressure on the rate of oxidation was determined by means of abrupt changes in  $P_{\text{O}_2}$  in the course of oxidation experiments (figure 3). In order to reach rapidly the Part 2 of the mass gain (higher than 15 g/m<sup>2</sup>), a  $2.5 \times 10^4$  Pa oxygen partial pressure was applied to the system. This pressure was chosen since it has been observed that the higher the oxygen pressure, the higher the rate of oxidation in Part 1.

Subsequently, an initial sudden change of oxygen partial pressure to  $2.5 \times 10^2$  Pa was performed. After one hour in these conditions the cermet was submitted to a second abrupt change of oxygen partial pressure to variable values between  $2.5 \times 10^2$  and  $2.5 \times 10^4$  Pa.

After the oxygen pressure changes, the mass gain is linear, so the oxidation rate was deduced from the slope of the straight-line. Figure 4 represents the rate of oxidation as a function of the oxygen partial pressure which exhibits two kinetic regimes: the rate increases with the increasing oxygen partial pressure up to  $5 \times 10^3$  Pa; above this oxygen partial pressure, denoted  $P_{\text{Cu}}$ , the rate of oxidation becomes independent of this variable.

### SEM analysis

Microscopic observations of oxidized cermets show different characteristic zones represented in Figures 5a and 5b and denoted: C, P<sub>1</sub>, P<sub>2</sub>, E<sub>2</sub> and E<sub>1</sub> from the bulk to the surface of the material.

In Figure 5a, the innermost zone C appears to be very similar to the initial material, since the metallic particles are surrounded by nickel ferrite, and the nickel oxide does not contain any nickel ferrite precipitates. This means that no reaction has occurred in this part of the material.

Starting from C and going towards the surface, the next zone is P<sub>2</sub>. There, the metallic particles appear to be surrounded by a layer of nickel oxide, which seems to develop at the expense of the nickel ferrite (Figure 6, labels a and c). Numerous observations indicate that this nickel oxide phase appears systematically on the side nearest to the oxidizing atmosphere. Moreover, in zone P<sub>2</sub> some metallic particles have disappeared, creating voids and thus increasing porosity (Figure 6, label b).

Corrosion Science, 2009, 51(4), 752-760, [doi:10.1016/j.corsci.2009.01.019](https://doi.org/10.1016/j.corsci.2009.01.019)

Zone P<sub>1</sub> (Figure 5a) appears to be less porous than zone P<sub>2</sub>. There are no metal particles and the nickel oxide phase contains ferrite precipitates (Figure 6, label d). Zone E<sub>2</sub> is a layer of nickel oxide (figure 6, label e). Finally, zone E<sub>1</sub> is a copper oxide scale, the composition of which depends on the applied oxygen partial pressure (Figure 6, label f). Tenorite (CuO) is the outermost layer above 5.10<sup>3</sup> Pa and cuprite (Cu<sub>2</sub>O) is the outermost layer below this value (Figures 7a and b).

It can be observed from samples oxidized for various durations that the E<sub>1</sub> and E<sub>2</sub> layers grow continuously.

Gold droplets deposited on the initial surface can be observed in Figure 8. They are mainly localized at the E<sub>2</sub>/P<sub>1</sub> interface, which corresponds to the initial surface of the disk. Few droplets can be observed in other areas, probably due to the metallographic preparation. Consequently, it can be deduced that E<sub>1</sub> and E<sub>2</sub> are externally grown oxides (outward development from the initial surface). In the following, the term “external” will refer to these two layers. For any oxidized sample, the mass gain due to these external layers can be calculated and compared to the total mass gain measured by thermogravimetry. Therefore, several samples were oxidized during various periods in the thermobalance and observed in order to determine the extent of zones changes, the total mass gain and the mass gain due to the outermost oxide scales. Figure 9 shows the plot of the mass gain calculated from the thickness of the surface layers, versus the mass gain measured by thermogravimetry. This graph clearly shows that the mass gain due to oxygen fixed by the external oxides is lower than the total reacting oxygen.

### EPMA analysis

Quantitative EPMA analyses have been done on a cermet, oxidized at 960°C for 30 hours and in 8.10<sup>4</sup> Pa of oxygen. Figure 10 represents the various areas that were analyzed, and Figure 11 displays the corresponding concentration profiles of Cu, Ni, Fe and O elements in each phase. From these analyses, numerous observations can be made:

- copper is the only cation composing the outmost surface layer, E<sub>1</sub>. In this case, CuO was identified.
- all the different cations are present in E<sub>2</sub>, a similar phase composition can also be observed in zone P<sub>1</sub>.
- in P<sub>1</sub>, the nickel ferrite phase contains up to 5%wt of copper (the weight percentage corresponds to the mass of copper over the mass of all the elements in the phase, cations and anions).
- in P<sub>2</sub>, where metallic particles still subsist, the closer the metal phase is to the interface P<sub>1</sub>/P<sub>2</sub>, the less nickel it contains.
- considering the nickel ferrite composition, from C to P<sub>1</sub>, the Fe concentration decreases and a small amount of copper is inserted into the nickel ferrite phase: the composition goes from Ni<sub>0,8</sub>Fe<sub>2,2</sub>O<sub>4</sub> to Ni<sub>0,87</sub>Cu<sub>0,18</sub>Fe<sub>1,95</sub>O<sub>4</sub> for the bulk and the oxidized zone respectively,
- the Ni concentration decreases in the nickel oxide phase, and copper insertion into the cubic structure occurs. The chemical composition in zone C is Ni<sub>0,84</sub>Fe<sub>0,16</sub>O, whereas in P<sub>1</sub> it was measured to be Ni<sub>0,59</sub>Cu<sub>0,29</sub>Fe<sub>0,12</sub>O.

### SIMS analysis

Figure 12 represents a SIMS analysis of the sample border where the four oxidized zones (E<sub>1</sub>, E<sub>2</sub>, P<sub>1</sub> and P<sub>2</sub>) can be observed. The outermost layer contains a lot of isotopic <sup>18</sup>O and represents E<sub>1</sub> and E<sub>2</sub>.

P<sub>1</sub> is a low porosity zone, which only contains oxides formed with <sup>18</sup>O or <sup>16</sup>O (cf. figure 12). In this zone, <sup>18</sup>O is not homogeneously distributed into the phases and seems to be mainly localized along grain boundaries and in few phases. All of the oxygen involved in the internal oxidation of the cermet (2/3 of the total mass gain) is contained in zone P<sub>1</sub>. Looking accurately at zone P<sub>1</sub>, phases containing <sup>18</sup>O can be identified (Figure 13, label a). The ‘Ni + O’ signal being far higher than the ‘Fe + O’ signal, this phase is a nickel oxide

Corrosion Science, 2009, 51(4), 752-760, [doi:10.1016/j.corsci.2009.01.019](https://doi.org/10.1016/j.corsci.2009.01.019) and not a nickel ferrite. Zone P<sub>1</sub> is composed of nickel ferrite and nickel oxide particles containing <sup>16</sup>O, but also of nickel oxide particles containing <sup>18</sup>O.

As mentioned previously, nickel ferrite precipitates appear in nickel oxide particles of zone P<sub>1</sub>, as shown by Label b in figure 13 (the ferrite precipitates can be easily identified by comparing the 'Fe + O' and 'Ni + O' signal images). Observations of <sup>18</sup>O signal in this zone show that the precipitates do not contain isotopic <sup>18</sup>O, but <sup>16</sup>O.

Deeper in the material, the innermost oxidized zone is P<sub>2</sub>. SEM and EPMA observations have shown that the composition of the alloy particles has been modified: they contain less nickel than the alloy particles of the initial material (or than the non-oxidized zone, C) and voids appear (Figure 6, label a and c). This is the result of nickel oxidation and copper diffusion towards the surface. Nickel is the first element to oxidize in the alloy particles. The resulting nickel oxide surrounds the remaining alloy particles (or voids if copper diffusion has already occurred), the corresponding SIMS analysis is given by Label a in figure 12. The comparison of the <sup>18</sup>O and <sup>16</sup>O signals for this area shows that this oxide contains <sup>16</sup>O and that no isotopic oxygen has reacted with the metallic nickel.

## Discussion

### Oxidation kinetics

The oxidation rate at 960°C increases with oxygen partial pressure up to approximately  $5 \times 10^3$  Pa ( $P_{Cu}$ ) and is independent of this parameter above this value (cf. Figure 4). SEM and EPMA observations also revealed that below this oxygen pressure the outermost oxide layer is cuprite while tenorite is the outermost oxide layer above this oxygen pressure. This is consistent with thermodynamic data<sup>5</sup>, which indicate that  $5.1 \times 10^3$  Pa corresponds to the equilibrium oxygen pressure at 960°C between the tenorite and cuprite phases, according to the reaction (1):



The oxidation of copper and copper-nickel alloys has been studied extensively<sup>6,7</sup>. Authors agree that the kinetics of copper oxidation is controlled by cation vacancy diffusion through Cu<sub>2</sub>O ( $V_{Cu_2O}$  and  $V_{Cu_2O}^{\times}$ ). Above  $P_{Cu}$ , the cuprite layer is covered by a layer of tenorite, which becomes the outermost layer on the oxidized copper sample (cf. figure 14). Consequently, irrespective of the gaseous oxygen partial pressure, above  $P_{Cu}$ , the CuO/Cu<sub>2</sub>O interface sets its equilibrium (oxygen pressure of  $5.1 \times 10^3$  Pa). This implies that the concentration of vacancies at the interface CuO/Cu<sub>2</sub>O is fixed by the equilibrium and that the diffusion of those defects via the cuprite layer (rate-limiting step of copper oxidation) is independent of the external oxygen pressure.

By analogy with the oxidation of copper, it may be suggested that the rate of oxidation becomes independent of the oxygen pressure due to the presence of a CuO/Cu<sub>2</sub>O interface, in the case of a rate-limiting step located below this interface (even though cuprite has not been observed in our system above  $P_{Cu}$ ).

In the following, we discuss the results of the microstructural observations in relation with the thermogravimetric study in order to explain qualitatively the changes due to oxidation.

### Mass gain repartition

Fully oxidized cermets disks have been analyzed by XRD, they contain only nickel oxide, nickel ferrite, and copper oxides. This means that the final material after oxidation will contain Ni (II), Fe (II) and (III), Cu (I) and (II). Copper, initially present in the metal phase will be oxidized into Cu (II) in nickel oxide, nickel ferrite and tenorite, and into Cu (I) in cuprite. Nickel is initially present in the metallic phase and Ni (II) is contained in nickel oxide and nickel ferrite. Only Ni (II) will exist in the final material in nickel ferrite and nickel oxide. Concerning iron, it is already present as Fe (II) and Fe (III) in nickel oxide (Ni,Fe)O and nickel ferrite, respectively, and thus Fe (II) ions can be oxidized into Fe (III). Estimation of the oxidation of metallic copper and nickel into Cu (II) and Ni (II) represents nearly 97% of the total measured mass gain. Consequently, the mass gain due

Corrosion Science, 2009, 51(4), 752-760, [doi:10.1016/j.corsci.2009.01.019](https://doi.org/10.1016/j.corsci.2009.01.019)  
to iron oxidation is negligible compared to the mass gain due to copper and nickel oxidation.

### Microstructure

#### ✓ External and internal oxidation

Five distinct zones have been identified in the oxidized samples, C, P<sub>1</sub>, P<sub>2</sub>, E<sub>2</sub> and E<sub>1</sub>. Gold markers allowed to determine that the two outmost layers (E<sub>2</sub> : nickel oxide and E<sub>1</sub> : copper oxide) grew by external oxidation.

The oxygen amount contained in those two oxides is less than the total amount of oxygen reacting during oxidation and measured by thermogravimetry. This implies that oxygen also diffuses into the material. More precisely, figure 9 indicates that two thirds of the oxygen consumed by the reaction diffuses into the material, and one third contributes to the growth of two external oxide layers. SIMS analysis of a sample oxidized with <sup>18</sup>O confirms that diffusion of isotopic oxygen has occurred in zone P<sub>1</sub>, as observed in figure 12. Nickel oxide and copper oxides are known to be non-stoichiometric oxides with cation vacancies. Spinel phases as nickel ferrite and iron oxide can contain, both, cation vacancies and interstitial cations<sup>8-15</sup>. The fact that all the phases contain cationic vacancies or interstitial cations as major defects implies that, for bulk diffusion, cation diffusion would be much more probable than anion diffusion. Consequently, diffusion via vacancies or interstitials would only lead to an external growth of oxides<sup>16</sup>, and the measured mass gain should correspond to the oxygen contained in the external layers formed during the reaction. This is in contradiction with the observed mass gain, indicating that grain boundary diffusion of oxygen might take place in the cermet. This is well put in evidence by SIMS observations (cf. figure 12). In zone P<sub>1</sub>, the isotopic oxygen is not homogeneously distributed into the phases and mostly appears at the grain boundaries. Then, cation flux from the inner part of the material and oxygen flux from the surface will both have to be considered to describe the cermet oxidation.

#### ✓ Zones formation mechanism

Zone P<sub>2</sub> is the closest zone to the center that has been affected by oxidation. SEM observation shows the simultaneous formation of voids and nickel oxide in contact with the remaining alloy (when not totally consumed) (cf. figure 6, label c). The nickel oxide surrounding the alloy particles or/and the voids of zone P<sub>2</sub> comes from the oxidation of the nickel initially contained in the alloy. This is suggested by EPMA analysis of the metallic particles that reveal a lower concentration of nickel in the alloy of this zone than in the alloy of the initial material (or in the non-oxidized zone, C).

Oxidation of nickel contained in the alloy requires oxygen that can be supplied either by the atmosphere via inwards diffusion or by reaction with the nickel ferrite phase. The nickel oxide would thus grow at the expense of the metal particles in the first case whereas in the second case, the reaction leads to the consumption of the nickel ferrite phase. SEM observation shows that the nickel ferrite is consumed by the nickel oxide (cf. figure 6, label c). Besides, SIMS results show that the nickel oxide surrounding the metallic particles is only composed of <sup>16</sup>O (cf. figure 12, label a). This implies that the metallic nickel reacted with the oxygen of an oxide initially contained in the material and in contact with the metallic phase.

Concerning the outermost layer (E<sub>1</sub>), its growth requires the diffusion of copper from the metallic particle towards the surface. Simultaneously the insertion of copper into nickel oxide and nickel ferrite phases occurs.

Reaction of nickel with the surrounding nickel ferrite and migration of copper towards the surface are both responsible for the formation of voids in zone P<sub>2</sub> and for the inward advance of the P<sub>2</sub>/C interface.

P<sub>1</sub> is a low porosity zone devoid of metallic particles and only composed of nickel ferrite and nickel oxide. Considering evolution of the material with time, this zone P<sub>1</sub> has previously been a P<sub>2</sub> type zone and submitted to the same phenomenon as described previously: voids were produced by nickel oxidation and copper diffusion. Subsequently

Corrosion Science, 2009, 51(4), 752-760, [doi:10.1016/j.corsci.2009.01.019](https://doi.org/10.1016/j.corsci.2009.01.019)

these pores were filled by oxides (ferrite nickel or nickel oxide) to create this low porosity zone. Considering that two thirds of the reacting oxygen must diffuse inwards to explain all the mass gain of the oxidation (as explained in section “external and internal oxidation”), voids must have been filled by oxides produced by the reaction between cations of the bulk and oxygen provided directly by the atmosphere. Nickel oxide particles containing  $^{18}\text{O}$  have been identified in zone  $P_1$  of the sample oxidized with isotopic oxygen (Figure 13, label a). They are certainly the particles that filled the voids left by the consumption of the metallic particles: it can be assumed that oxygen diffused from the surface of the sample into  $P_1$  via the grain boundaries, then reacted with cations contained in the material, to form a nickel oxide phase which filled the voids. This mechanism allows to understand the porosity disappearance in zone  $P_1$  and the advance inwards the sample of the interface  $P_1/P_2$ .

Ferrite nickel precipitates have also been observed in zone  $P_1$ . These are the result of Fe oxidation from Fe(II) to Fe(III) in nickel oxide due to two possible mechanisms. The first one is the diffusion of oxygen into the oxide: the cations contained in nickel oxide are immobile and oxygen diffuses inwards to produce nickel ferrite precipitates. The second one is a mechanism of internal oxidation of an oxide solid solution to a higher oxide via cation vacancies, which has been proposed by Schmalzried<sup>17</sup> (cf. figure 15). Reaction (2) describes the reaction between cation vacancies diffusing into a nickel oxide particle with cations and oxygen from this oxide:



Thus, cations diffuse towards the surface of the nickel oxide phase and the consequence is the formation of ferrite nickel precipitates.

If diffusion of oxygen (first mechanism) into the nickel oxide particles was responsible for the nickel ferrite precipitates formation,  $^{18}\text{O}$  would have been observed in the nickel ferrite precipitates of the sample oxidized with isotopic oxygen. On the contrary, SIMS analysis has revealed that those precipitates only contain  $^{16}\text{O}$  (Figure 13, label b).

Consequently, the mechanism of oxidation via cation vacancies is in a better agreement with the experimental observations.

$E_1$  and  $E_2$  are the results of external oxidation. Oxygen is adsorbed at the surface of the sample (on  $E_1$ ) and builds new copper oxide bricks ( $\text{CuO}$  or  $\text{Cu}_2\text{O}$ , depending on the oxygen partial pressure<sup>6</sup>). The consequence of this layer formation is the production of cation vacancies that diffuse into the material and allow the cations migration towards the surface. Similarly,  $E_2$  grows externally due to the consumption of oxygen of  $E_1$ .

Finally, the mechanism of oxidation of the material should account for the following reactions:

- ❖ outwards growth of  $\text{CuO}/(\text{Cu}_2\text{O})/(\text{NiFeCu})\text{O}$  because of cation diffusion via cation vacancies in the various oxide phases.
- ❖ NiO internal formation because of reaction between Cu-Ni particles and nickel ferrite phase.
- ❖ transient formation of voids (in  $P_2$ ).

## Conclusions

The rate of oxidation of a cermet composed with nickel ferrite ( $\text{Ni}_x\text{Fe}_{3-x}\text{O}_4$ ), nickel oxide ( $\text{Ni}_y\text{Fe}_{1-y}\text{O}$ ) and nickel-copper alloy ( $\text{Cu}_z\text{Ni}_{1-z}$ ) ( $x=0.8$ ;  $y=0.84$ ;  $z=0.44$ ) increases with the oxygen pressure below  $5.1 \times 10^3$  Pa. Above this value, tenorite appears at the surface of the sample and oxidation kinetics become independent of the oxygen pressure.

Weight gain of the samples during oxidation is the consequence of both external and internal oxidation. Two external layers, copper oxide and nickel oxide, correspond to one third of the total amount of oxygen consumed for the reaction and are the result of cationic vacancy diffusion. The remaining reacting oxygen diffuses into the material via the grain boundaries and accounts for the internal oxidation of the material.

## Acknowledgements

This work is sponsored by Alcan CRV and French “Ministère de l’Economie, des Finances et de l’Industrie” which are gratefully acknowledged.

SIMS analyses have been made by F. Horreard and A. Merkulov from CAMECA society. They are greatly acknowledged for their collaboration.

The authors want to acknowledge Prof. M. Soustelle, from Ecole Nationale Supérieure des Mines de Saint-Etienne, for fruitful discussions.

## References

- 1 R. Haugrud, T. Norby, P. Kofstad, “On the high temperature oxidation of Cu-30wt%Ni-15wt%Fe”, *Corrosion Science*, [43] 283-299 (2001).
- 2 US Patent 4399008, S.P. Ray, “Composition for inert electrodes”, Aluminum Company of America, (1980); US Patent 4374761, S.P. Ray, “Inert electrode formulation”, Aluminum Company of America, (1980); US Patent WO00044952, R.K. Dawless, R.B. Hosler, S.P. Ray, “Inert electrode containing metal oxides, copper and noble metal”, Alcoa, (1999).
- 3 M. Tupin, M. Pijolat, F. Valdivieso, M. Soustelle, A. Frichet, P. Barberis, “Kinetic study of the oxidation by oxygen of a zirconium based alloy: Zy-4, difference between the pre- and post-transition stages”, *J. Nucl. Mat* [317] 130-144 (2003).
- 4 P. Sarrazin, A. Galerie, J. Fouletier, pp 68-69 in “Les mécanismes de la corrosion sèche” (Dry corrosion mechanisms), Edited by EDP Science, 2000.
- 5 FactSage System, 2004, [www.factsage.com](http://www.factsage.com)
- 6 R. Haugrud, P. Kofstad, “On the oxygen pressure dependence of high temperature oxidation of copper”, *Material Science Forum*, [251-254] 65-72 (1997).
- 7 R. Haugrud, P. Kofstad, “On the high temperature oxidation of Cu-rich Cu-Ni alloys”, *Oxid. of Metals*, [50] 189-213 (1998).
- 8 K. Tsukimura, S. Sasaki, N. Kimizuka, “Cation distributions in nickel ferrites”, *Jpn. J. Appl. Phys.*, [36] 3609-3612 (1997).
- 9 W. Chul Kim, S. Jin Kim, S. Wha Lee, S. Hee Ji, “Atomic migration and superexchange interaction in  $\text{Ni}_{0.1}\text{Cu}_{0.9}\text{Fe}_2\text{O}_4$ ”, *IEEE transactions on magnetics*, [36] 3399-3401 (2000).
- 10 M. N. Khan, A. Memon, S. Al-Dallal, “Structural, electrical and spectroscopic studies of the system  $\text{Ni}_{1-x}\text{Cu}_x\text{Fe}_2\text{O}_4$ ”, *Int. J. Electronics*, [76] 953-959 (1994).
- 11 F. Haab, Th. Burhmaster, M. Martin, “High temperature in situ X-ray absorption studies on the iron valence in iron doped nickel oxide ( $\text{Ni}_{1-x}\text{Fe}_x$ ) $_{1-\phi}\text{O}$ ”, *Solid State Ionics*, [141-142] 289-293 (2001).
- 12 W.C. Tripp, N.M. Tallan, “Gravimetric determination of defect concentration in NiO”, *J. Am. Ceram. Soc.*, [53] 531-533 (1970).
- 13 F.A. Kröger, pp 406-418 in “The chemistry of imperfect crystals”, Edited by North-Holland Publishing Company, Amsterdam, 1964.
- 14 N. L. Peterson, W.K. Chen, D. Wolf, “Correlation and isotope effects for cation diffusion in magnetite”, *J. Phys. Chem. Solids* [41] 709-719 (1980).
- 15 S.H. Kang, H.I. Yoo, “Nonstoichiometry and high-temperature thermodynamic properties of ( $\text{Mg}_{0.22}\text{Mn}_{0.07}\text{Fe}_{0.71}$ ) $_{3-d}$  ferrite spinel”, *J. of Solid State Chem.*, [145] 276-282 (1999).
- 16 P. Kofstad, pp 162-240 in “High temperature corrosion”, Edited by Elsevier Applied Science, London and New York, 1988.
- 17 H. Schmalzried, pp 211-217 in “Chemical kinetics of solids”, Edited by VCH, Weinheim, 1995.

**Figure captions :**

Figure 1: BSE micrograph of non-oxidized Cu-Ni based cermet with (a) Cu-Ni alloy particle, (b) non-stoichiometric nickel ferrite, (c) nickel oxide (Ni,Fe)O.

Figure 2: Specific weight gain versus time for 1600 minutes of oxidation at 960°C under  $10^5$  Pa of oxygen.

Figure 3: Sudden change of oxygen partial pressure to variable values between  $2.5 \cdot 10^2$  and  $2.5 \cdot 10^4$  Pa on cermet materials. A  $2.5 \cdot 10^4$  Pa oxygen partial pressure was applied to the system in order to reach rapidly the part 2 of the mass gain (higher than  $15 \text{ g/m}^2$ ), then a first sudden change of oxygen partial pressure to  $2.5 \cdot 10^2$  Pa was performed. After one hour in these conditions the cermet was submitted to a second sudden change of oxygen partial pressure.

Figure 4: Rate of oxidation as a function of the oxygen partial pressure. The oxidation rate is given by the slope of the mass gain curve  $m(t)$  (second sudden change of oxygen pressure in figure 3), just after the oxygen pressure change.

Figure 5: BSE micrograph of a polished cross section of a cermet disk oxidized at 960°C during 164 hours in  $4.8 \cdot 10^2$  Pa of oxygen. C, P<sub>1</sub> and P<sub>2</sub> zones are represented on (a). E<sub>1</sub> and E<sub>2</sub> are represented on (b).

Figure 6: BSE micrograph of a polished cross section of a cermet disk oxidized at 960°C during 18 hours in  $10^5$  Pa of oxygen. It shows a Cu-Ni alloy particle surrounded by nickel oxide (a), porosity formation (b), metal phase surrounded by a nickel oxide phase that consumes nickel ferrite phase (c), nickel oxide phase that contain ferrite precipitates (d) and a layer of nickel oxide (e).

Figure 7: BSE micrographs of a polished cross section of cermet disks oxidized at 960°C during 16 hours in  $7 \cdot 10^2$  Pa of oxygen, where the outmost layer is Cu<sub>2</sub>O (a) and during 48 hours in  $2 \cdot 10^4$  Pa of oxygen, where the outmost layer is CuO (b).

Figure 8: BSE micrographs of a polished cross section of a cermet disk oxidized at 960°C during 24 hours in  $10^5$  Pa of oxygen.

Figure 9: Calculated external mass gain by thickness measurement of the external layers versus mass gain measured by thermogravimetry. The samples were oxidized at 960°C in  $10^5$  Pa of oxygen.

Figure 10: BSE micrograph (a) of a polished cross section of a cermet disk oxidized during 16 hours in  $2 \cdot 10^4$  Pa of oxygen at 960°C, and corresponding quantitative EPMA cartography of nickel (b), iron (c) and copper (d).

Figure 11: BSE micrograph (a) of a polished cross section of a cermet disk oxidized during 16 hours in  $2 \cdot 10^4$  Pa of oxygen at 960°C, and corresponding element concentration profiles from EPMA for of nickel oxide (b), metal (c) and nickel ferrite (d) phases.

Figure 12: SIMS analysis of the section of a cermet disk oxidized 24 hours in 990 hPa Ar and 10 hPa of <sup>18</sup>O. It shows the 4 different oxidized zones: E<sub>1</sub>, E<sub>2</sub>, P<sub>1</sub> and P<sub>2</sub>. (a) represents an alloy particle or a void surrounded by a nickel oxide layer.

Figure 13: SIMS analysis of zone P<sub>1</sub> of the section of a cermet disk oxidized 24 hours in 990 hPa Ar and 10 hPa of <sup>18</sup>O. (a) represents nickel oxide containing <sup>18</sup>O. (b) represents nickel oxide, composed of <sup>16</sup>O and containing nickel ferrite precipitates.

Figure 14: Oxidation of copper at 960°C in oxygen with a partial oxygen pressure above  $5.1 \cdot 10^3$  Pa.

Figure 15: Ferrite nickel precipitates formation in a nickel oxide particle. Mechanism of internal oxidation of nickel oxide via cation vacancies.

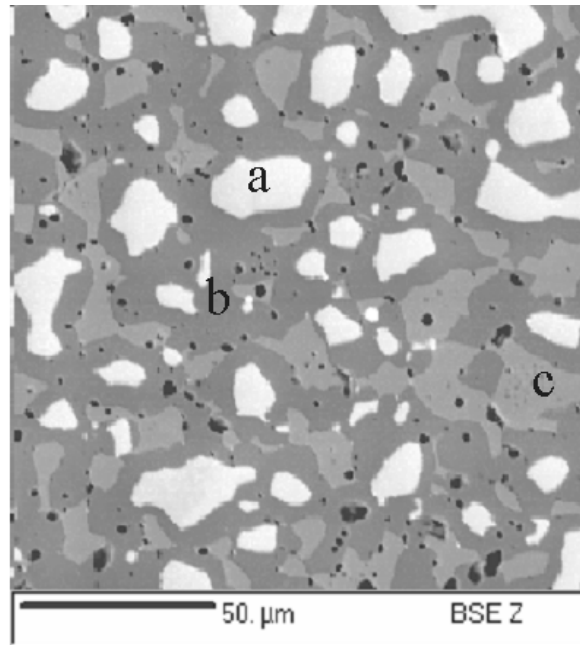


Figure 1: BSE micrograph of non-oxidized Cu-Ni based cermet with (a) Cu-Ni alloy particle, (b) non-stoichiometric nickel ferrite, (c) nickel oxide (Ni,Fe)O.

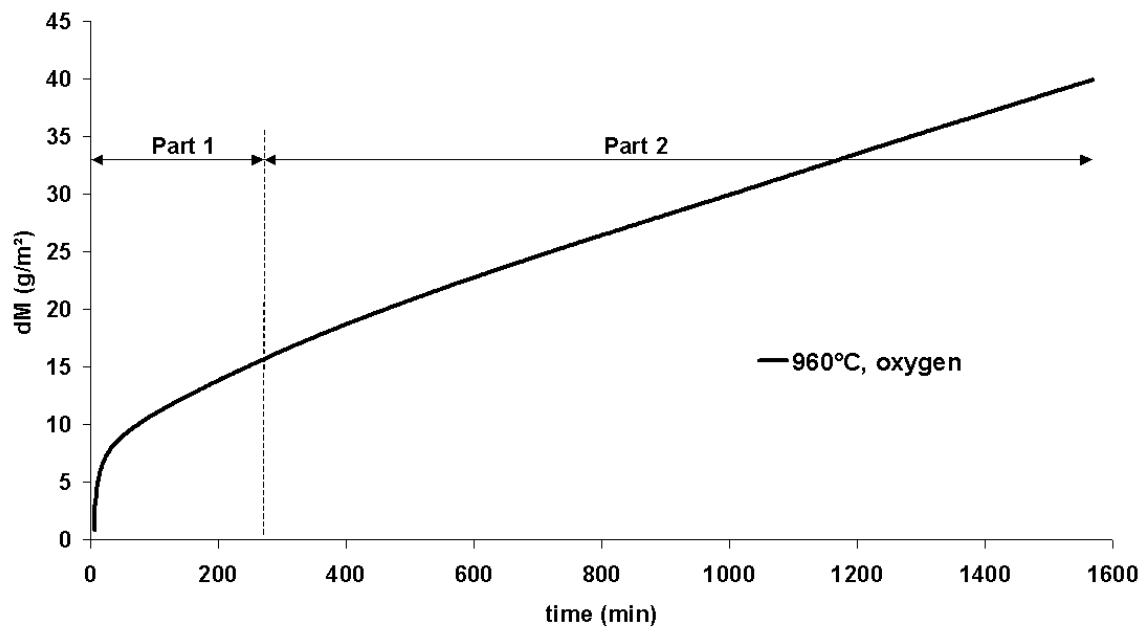


Figure 2: Specific weight gain versus time for 1600 minutes of oxidation at 960°C under  $10^5$  Pa of oxygen.

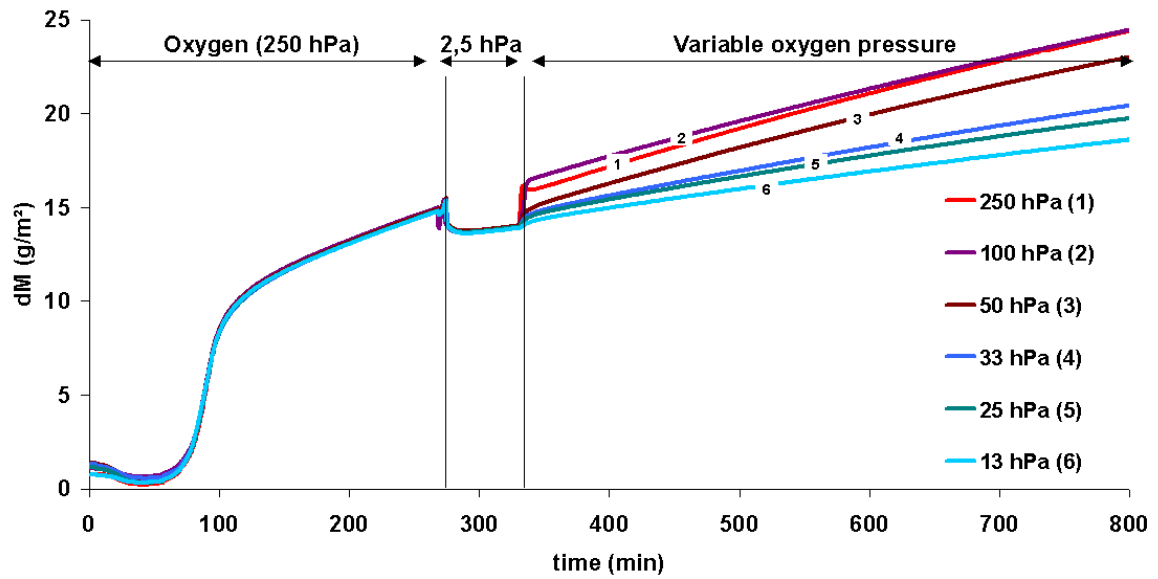


Figure 3: Sudden change of oxygen partial pressure to variable values between  $2.5 \cdot 10^2$  and  $2.5 \cdot 10^4$  Pa on cermet materials. A  $2.5 \cdot 10^4$  Pa oxygen partial pressure was applied to the system in order to reach rapidly the part 2 of the mass gain (higher than  $15 \text{ g/m}^2$ ), then a first sudden change of oxygen partial pressure to  $2.5 \cdot 10^2$  Pa was performed. After one hour in these conditions the cermet was submitted to a second sudden change of oxygen partial pressure.

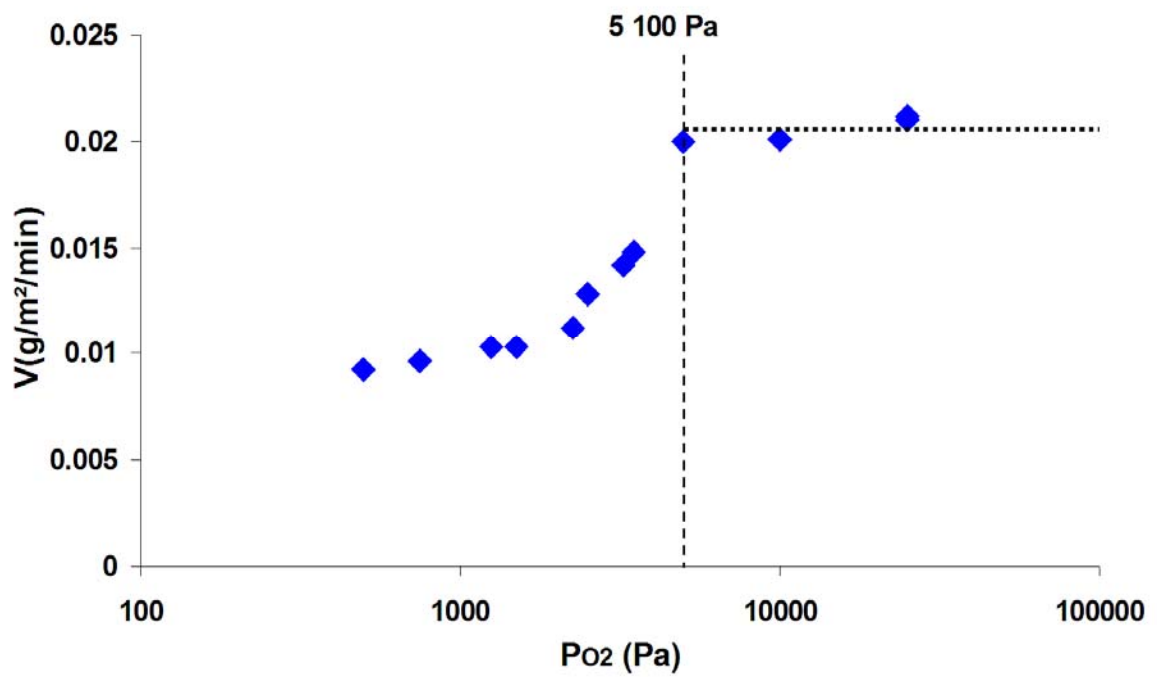


Figure 4: Rate of oxidation as a function of the oxygen partial pressure. The oxidation rate is given by the slope of the mass gain curve  $m(t)$  (second sudden change of oxygen pressure on figure 3), just after the oxygen pressure change.

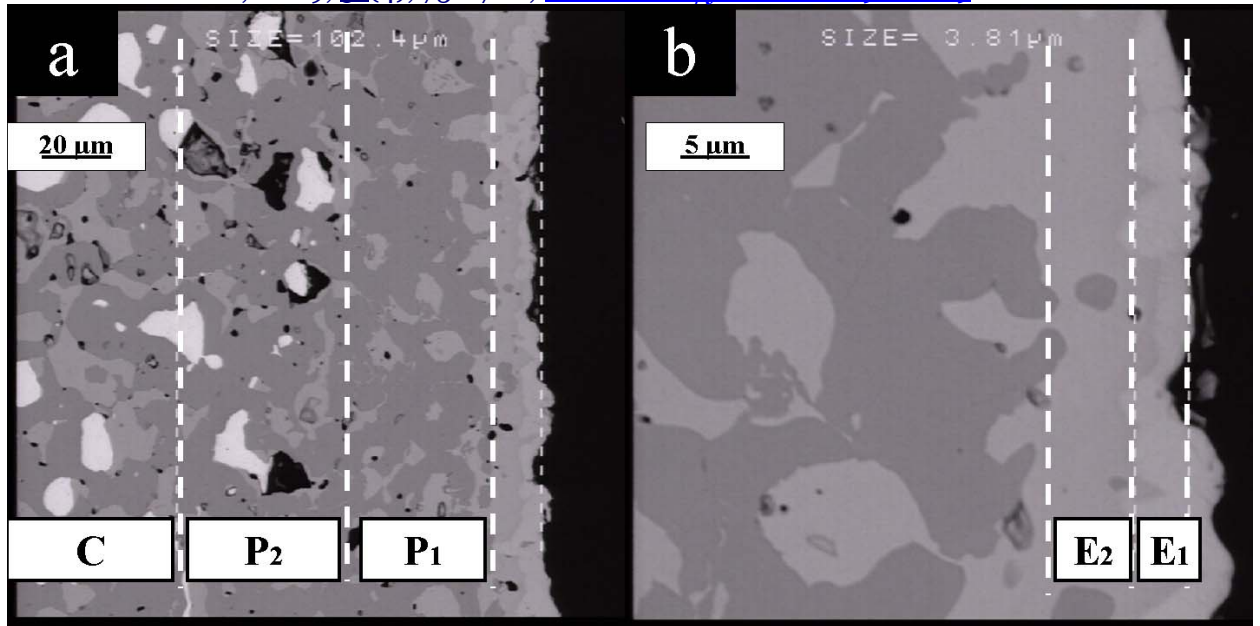


Figure 5: BSE micrograph of a polished cross section of a cermet disk oxidized at 960°C during 164 hours in 4.8 10<sup>2</sup> Pa of oxygen. C, P<sub>1</sub> and P<sub>2</sub> zones are represented on (a). E<sub>1</sub> and E<sub>2</sub> are represented on (b).

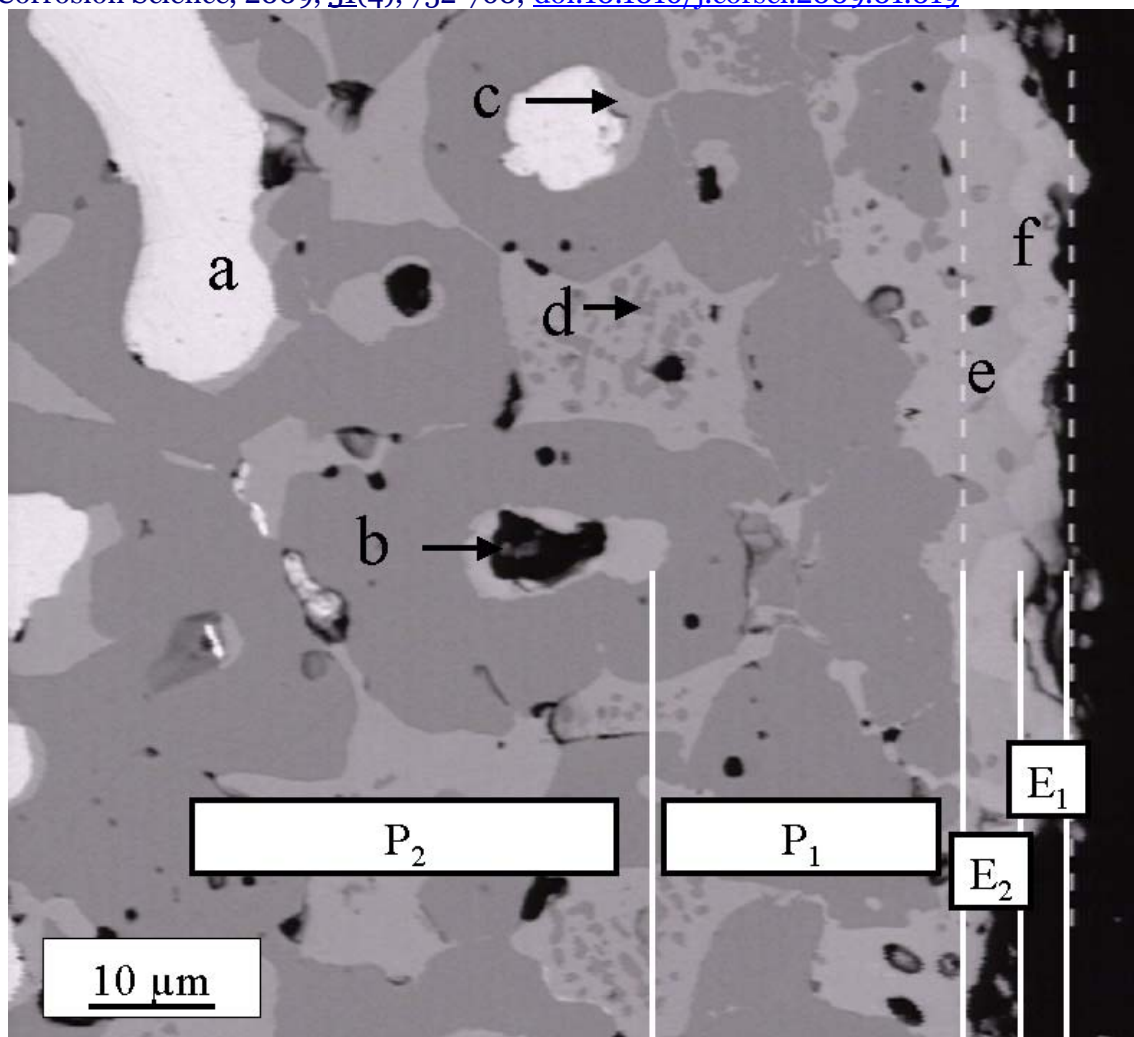


Figure 6: BSE micrograph of a polished cross section of a cermet disk oxidized at 960°C during 18 hours in  $10^5$  Pa of oxygen. It shows a Cu-Ni alloy particle surrounded by nickel oxide (a), porosity formation (b), metal phase surrounded by a nickel oxide phase that consumes nickel ferrite phase (c), nickel oxide phases that contain ferrite precipitates (d) and a layer of nickel oxide (e).

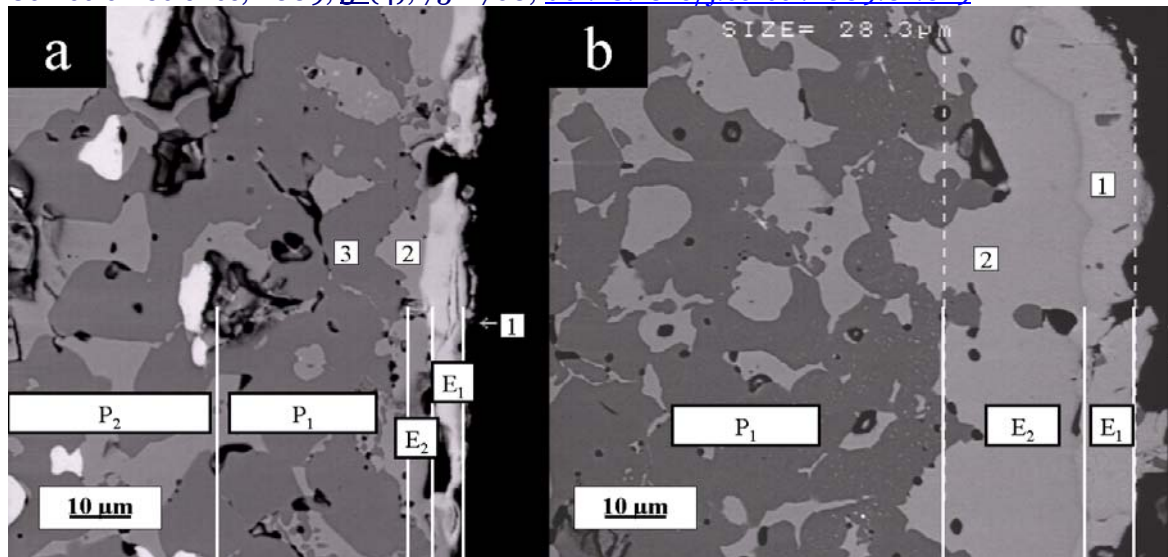


Figure 7: BSE micrographs of a polished cross section of cermet disks oxidized at 960°C during 16 hours in  $7 \cdot 10^2$  Pa of oxygen, where the outmost layer is  $\text{Cu}_2\text{O}$  (a, label 1) and during 48 hours in  $2 \cdot 10^4$  Pa of oxygen, where the outmost layer is  $\text{CuO}$  (b, label 1).

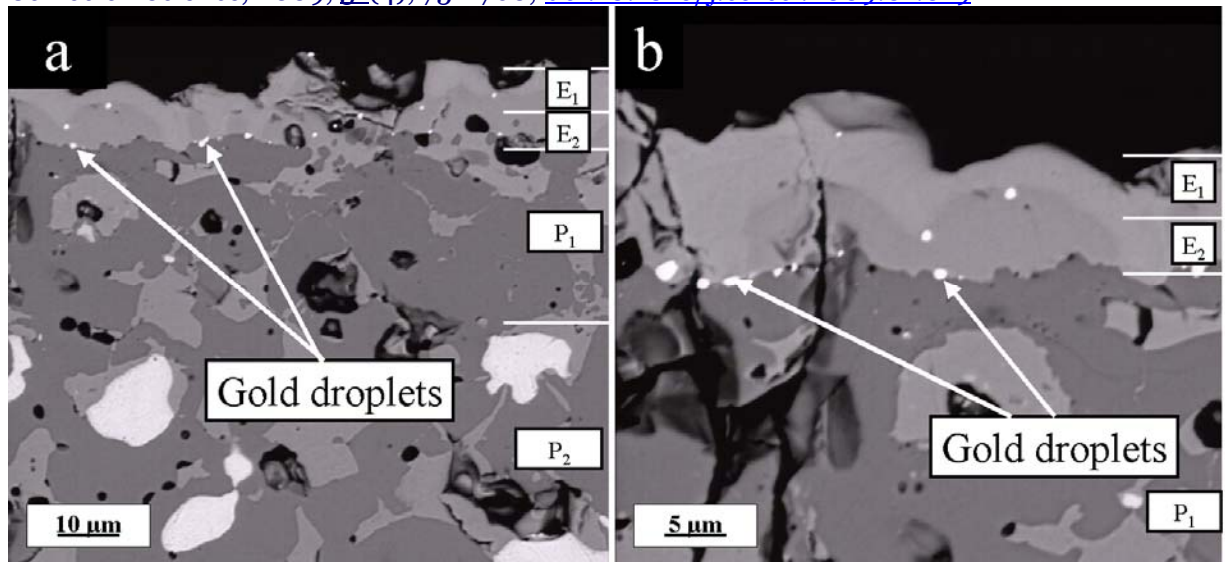


Figure 8: BSE micrographs of a polished cross section of a cermet disk oxidized at 960°C during 24 hours in 10<sup>5</sup> Pa of oxygen.

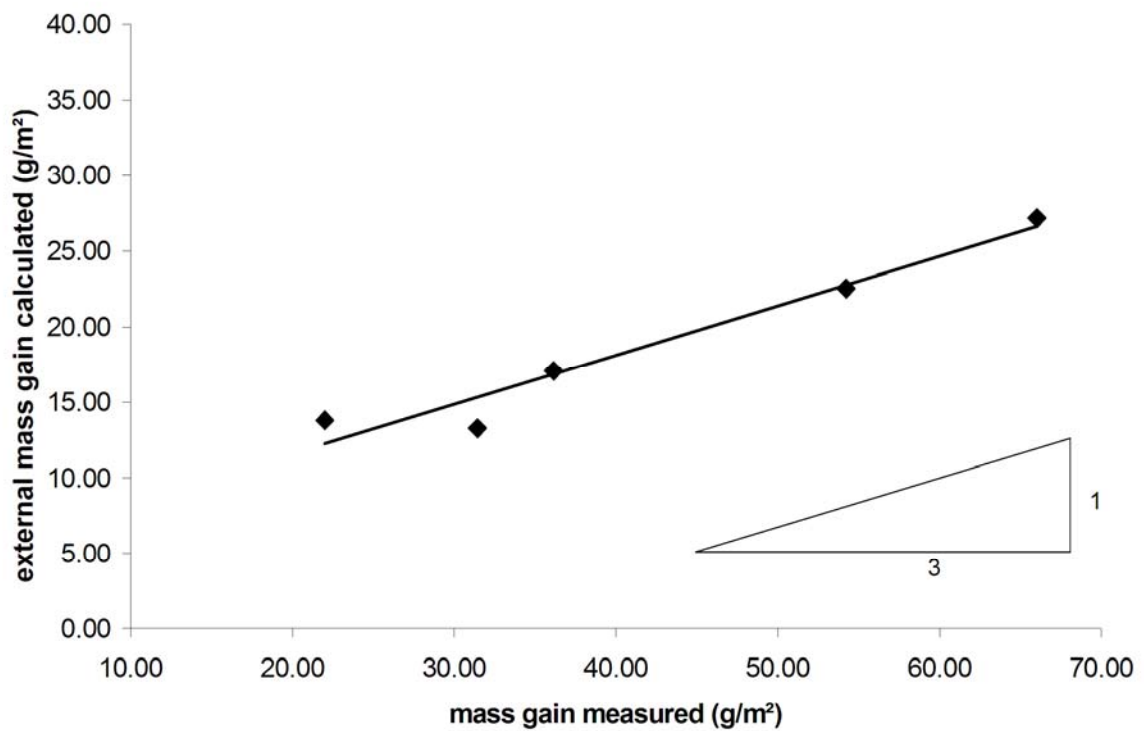


Figure 9: Calculated external mass gain by thickness measurement of the external layers versus mass gain measured by thermogravimetry. The samples were oxidized at 960°C in 10<sup>5</sup> Pa of oxygen.

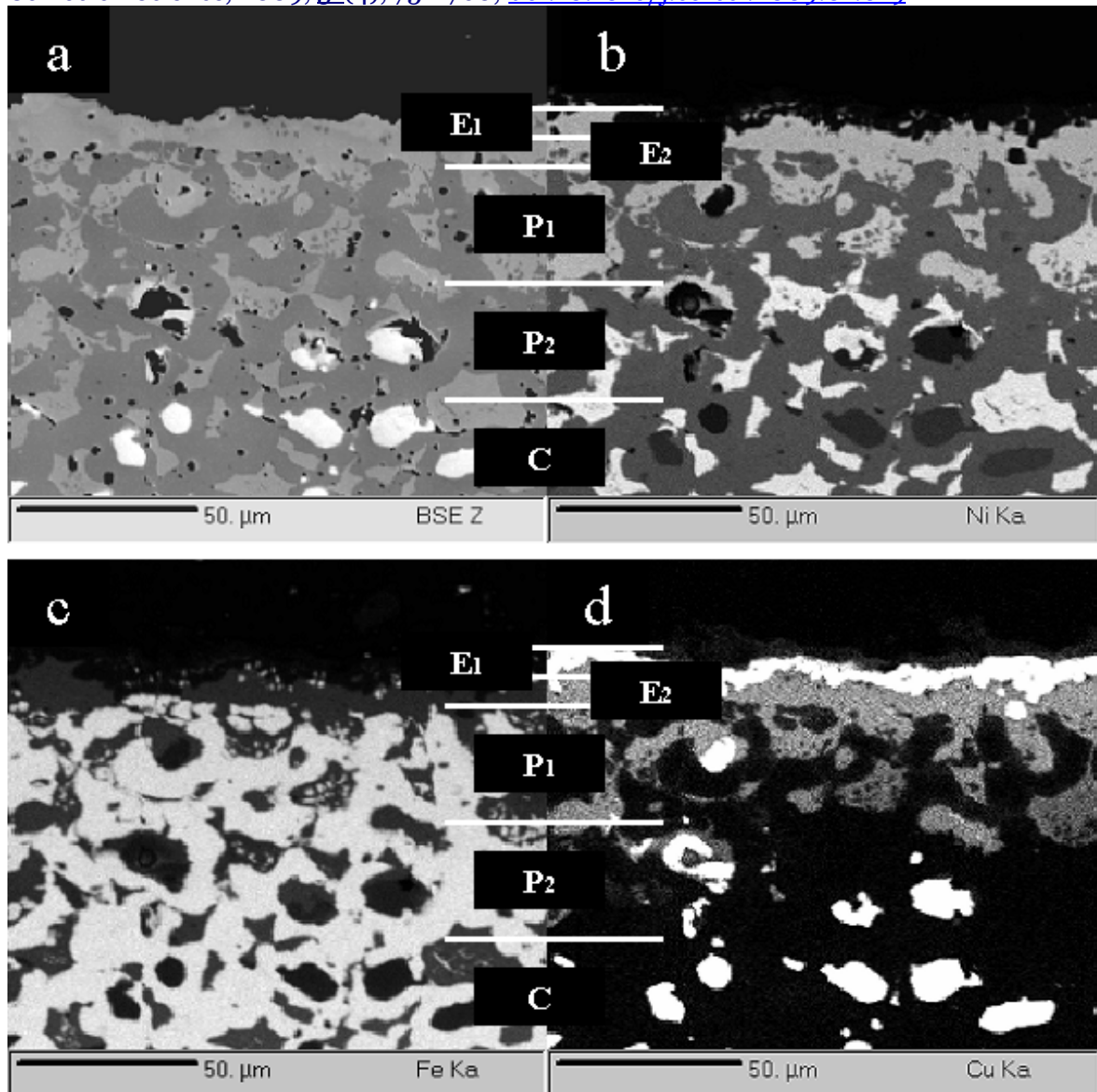


Figure 10: BSE micrograph (a) of a polished cross section of a cermet disk oxidized during 16 hours in  $2 \cdot 10^4$  Pa of oxygen at  $960^\circ\text{C}$ , and corresponding quantitative EPMA cartography of nickel (b), iron (c) and copper (d).

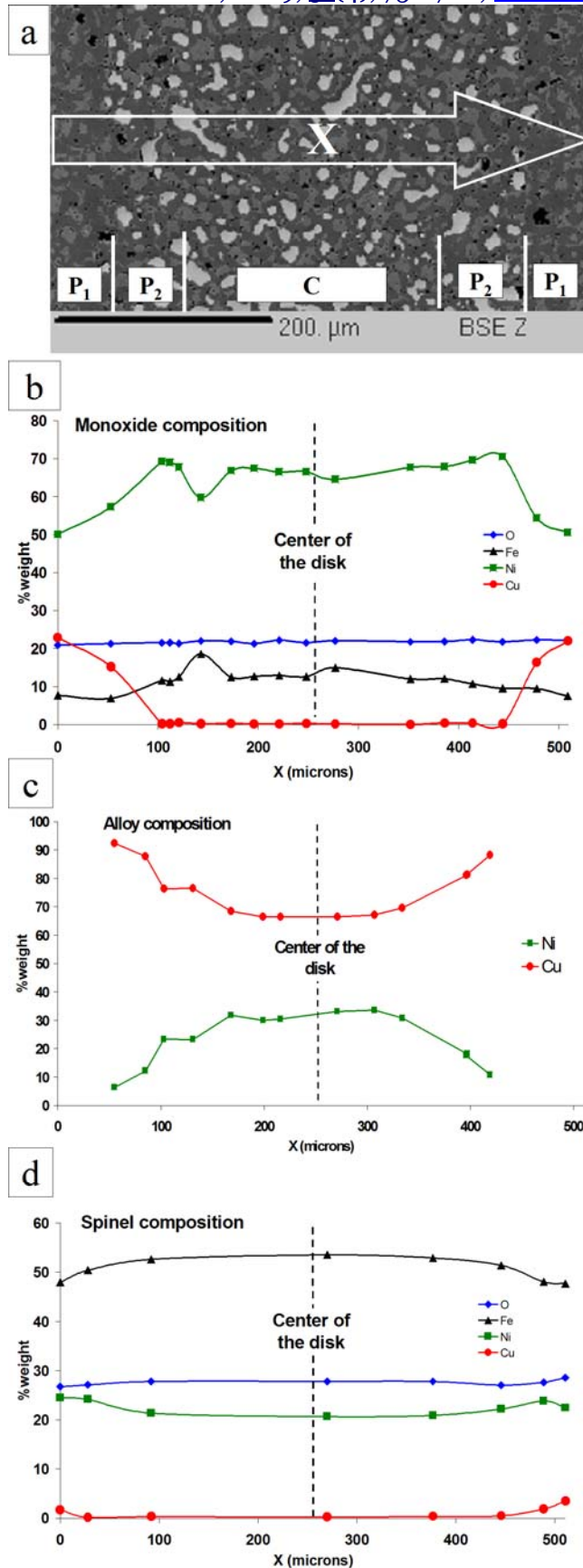
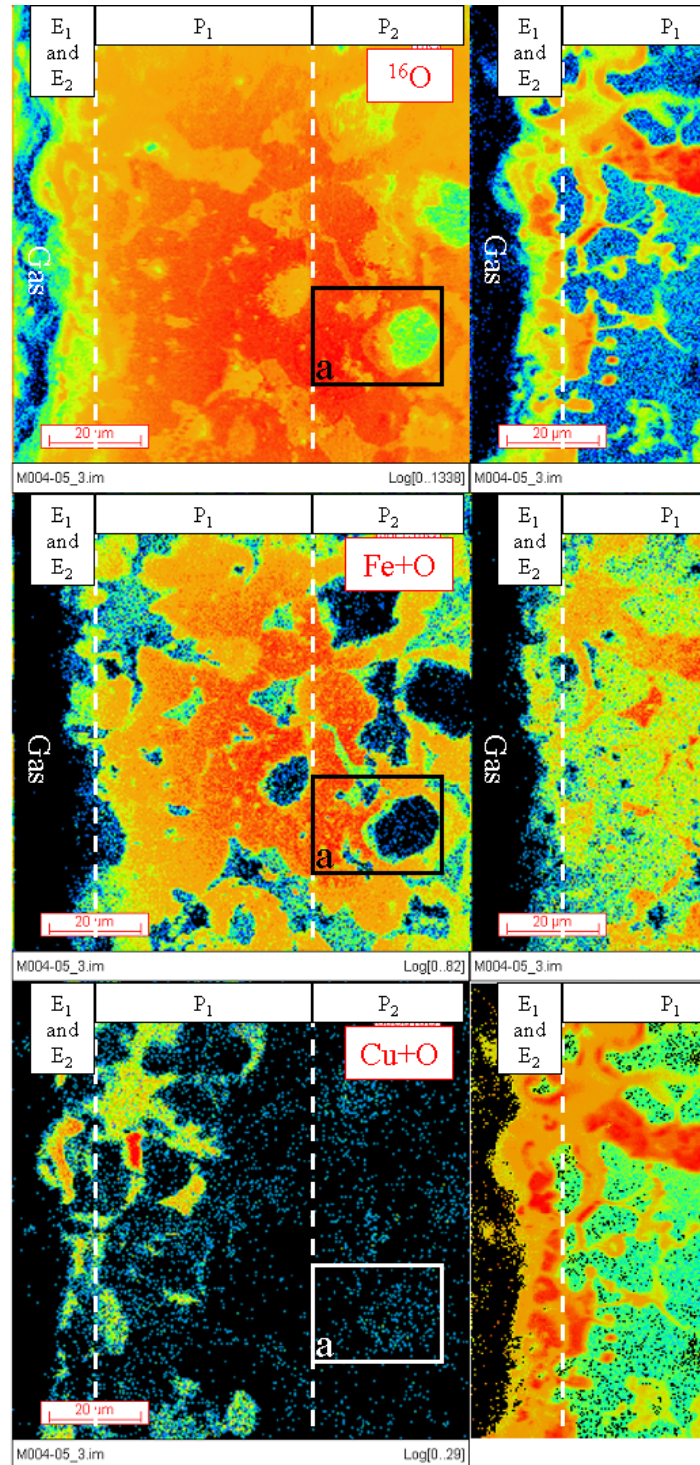


Figure 11: BSE micrograph (a) of a polished cross section of a cermet disk oxidized during 16 hours in  $2 \cdot 10^4$  Pa of oxygen at  $960^\circ\text{C}$ , and corresponding element concentration profiles from EPMA for nickel oxide (b), metal (c) and nickel ferrite (d) phases. ■ Ni; ● Cu; ▲ Fe; ◆ O.



Corrosion Science, 2009, 51(4), 752-760, [doi:10.1016/j.corsci.2009.01.019](https://doi.org/10.1016/j.corsci.2009.01.019)

Figure 12: SIMS analysis of the section of a cermet disk oxidized 24 hours in 990 hPa Ar and 10 hPa of  $^{18}\text{O}$ . It shows the 4 different oxidized zones: E<sub>1</sub>, E<sub>2</sub>, P<sub>1</sub> and P<sub>2</sub>. (a) represents an alloy particle or a void surrounded by a nickel oxide layer.

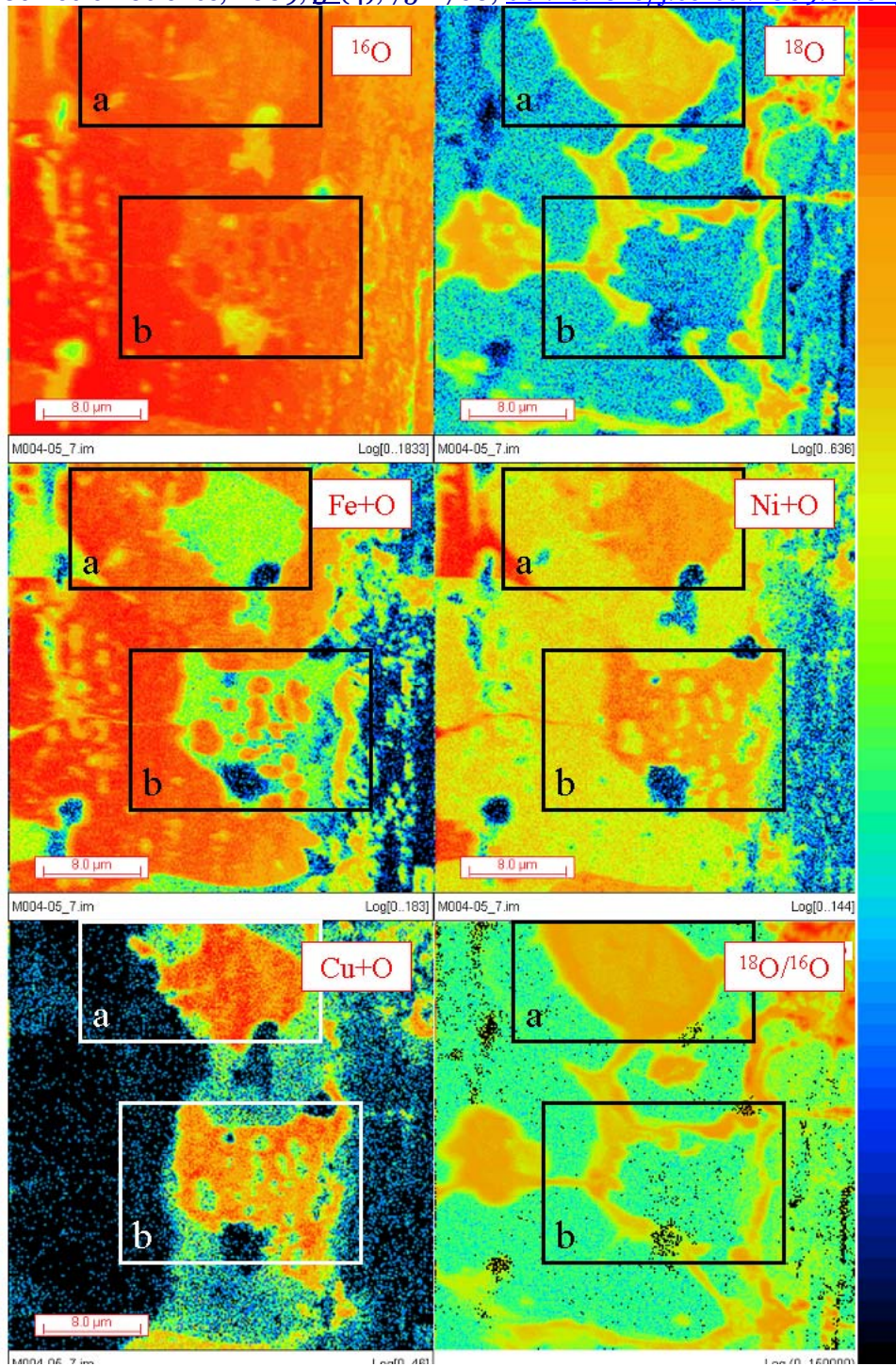


Figure 13: SIMS analysis of zone  $P_1$  of the section of a cermet disk oxidized 24 hours in 990 hPa Ar and 10 hPa of  $^{18}\text{O}$ . (a) represents nickel oxide containing  $^{18}\text{O}$ . (b) represents nickel oxide, composed of  $^{16}\text{O}$  and containing nickel ferrite precipitates.

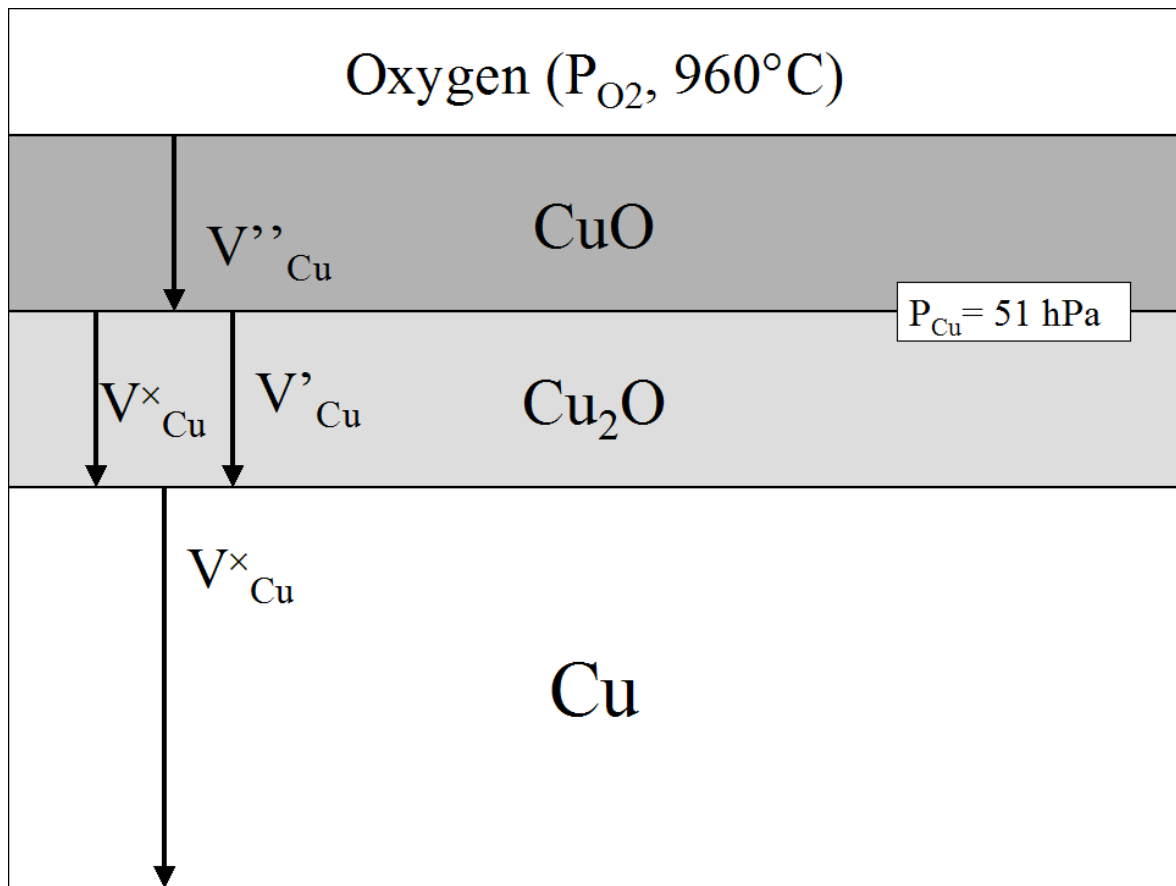


Figure 14: Oxidation of copper at 960°C in oxygen with a partial oxygen pressure above  $5.1 \cdot 10^3 \text{ Pa}$ .

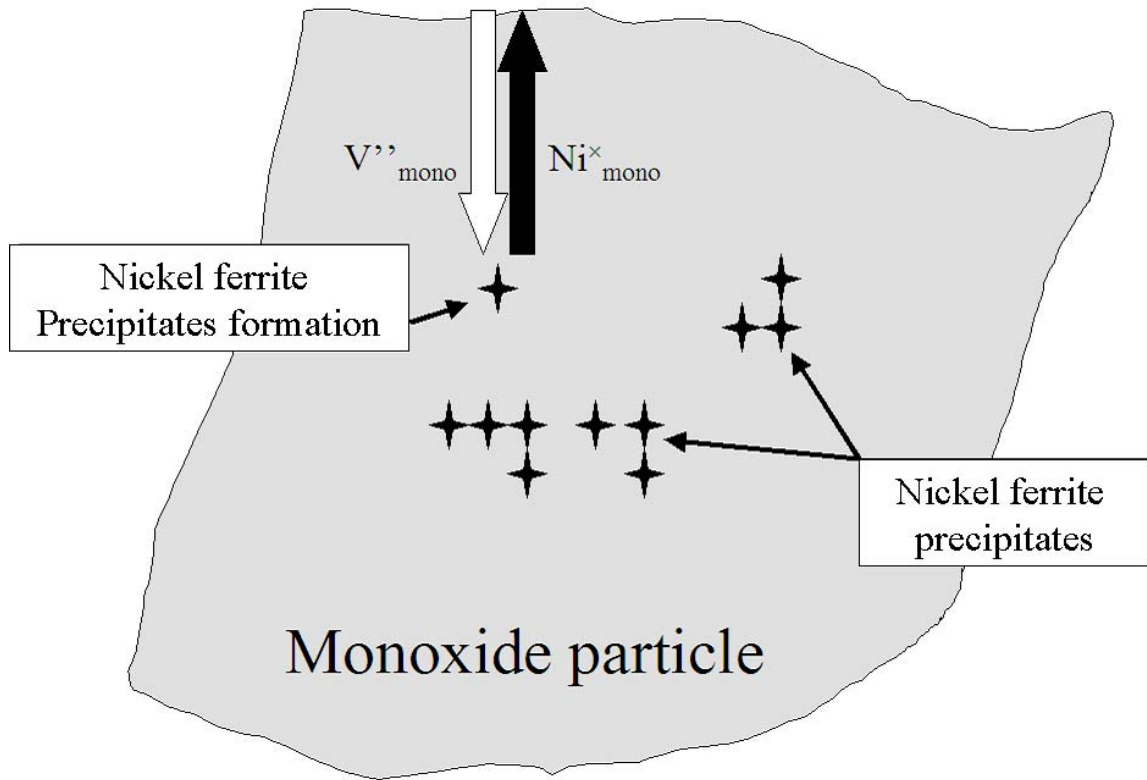


Figure 15: Ferrite nickel precipitates formation in a nickel oxide particle. Mechanism of internal oxidation of nickel oxide via cation vacancies.